

In Vivo Biodistribution of Engineered Lipid Microbubbles in Rodents

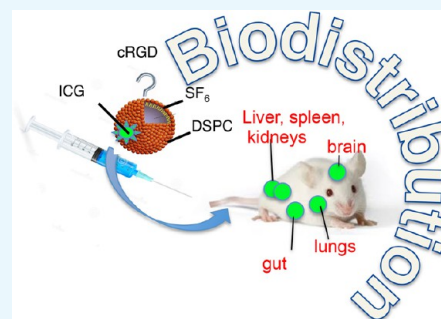
Letizia Oddo,[‡] Gaio Paradossi,[‡] Barbara Cerroni,[‡] Carmit Ben-Harush,[†] Eti Ariel,[†] Francesco Di Meco,[§] Zvi Ram,[†] and Rachel Grossman^{*,†}

[†]Department of Neurosurgery, Tel Aviv Medical Center, affiliated to the Sackler Faculty of Medicine, Tel-Aviv University, 6997801 Tel-Aviv, Israel

[‡]Dipartimento di Scienze e Tecnologie Chimiche, Università degli Studi di Roma Tor Vergata, 00133 Roma, Italy

[§]Neuro-Oncology Unit, Fondazione IRCCS Istituto Neurologico Carlo Besta, 20133 Milan, Italy

ABSTRACT: Maximal resection of intrinsic brain tumors is a major prognostic factor for survival. Real-time intraoperative imaging tools, including ultrasound (US), are crucial for maximal resection of such tumors. Microbubbles (MBs) are clinically used in daily practice as a contrast agent for ultrasound and can be further developed to serve combined therapeutic and diagnostic purposes. To achieve this goal, we have developed novel MBs conjugated to specific ligands to receptors which are overexpressed in brain tumors. These MBs are designed to target a tumor tissue, visualize it, and deliver therapeutic molecules into it. The objective of this study was to assess the biodistribution of the test items: We used MBs labeled with indocyanine green (MB-ICG) for visualization and MBs conjugated to a cyclic molecule containing the tripeptide Arg-Gly-Asp (RGD) labeled with ICG (MB-RGD-ICG) to target brain tumor integrins as the therapeutic tools. Male Sprague Dawley rats received a single dose of each MB preparation. The identification of the MB in various organs was monitored by fluorescence microscopy in anesthetized animals as well as real-time US for brain imaging. Equally sized control groups under identical conditions were used in this study. One control group was used to establish fluorescence background conditions (ICG), and two control groups were used to test autofluorescence from the test items (MBs and MB-RGD). ICG with or without MBs (naked or RGD-modified) was detected in the brain vasculature and also in other organs. The pattern, duration, and intensity of the fluorescence signal could not be differentiated between animals treated with ICG alone and animals treated with microbubbles MBs-ICG or MBs-RGD-ICG. Following MB injection, either naked or combined with RGD, there was a sharp rise in the Doppler signal within seconds of injection in the brain. The signal was mainly located at the choroid plexus, septum pellucidum, and the meninges of the brain. The signal subsided within a few minutes. Injection of saline or ICG alone to respective animals did not result in a similar raised signal. Following a single intravenous administration of MB-ICG and MB-RGD-ICG to rats, the MBs were found to be effectively present in the brain.



INTRODUCTION

Gliomas represent approximately one-third of all primary brain tumors¹ characterized by an infiltrative growth pattern into the brain parenchyma. Glioblastoma is the most common and deadliest malignant tumor of the central nervous system (CNS) with a median survival of only 14 months² and a 5 year survival rate of 5.5%.³ Surgery is the first step in a multimodal therapy for malignant glioma. The extent of resection is a key surgical outcome variable for reducing tumor recurrence and improving symptom management, quality of life, progression-free survival, and overall survival in glioma patients.^{2,4–10} However, it is well known that tumor margins, due to their infiltrative growth, are difficult to depict. While complete surgical resection of these infiltrative tumors is often hampered by the absence of intraoperative real-time imaging, more surgical tools are emerging to assist neurosurgeons to identify the tumor's boundaries during surgery. Existing surgical modalities, such as intraoperative neuronavigation, 5-aminolevulinic acid (5-ALA) fluorescence-guided tumor resection, and intraoperative magnetic resonance imaging (MRI), while allowing the surgeon to

evaluate intraoperatively the extent of resection, all have their own limitations.^{9,10} A limitation of standard frameless stereotactic navigation is the lack of an updated navigational dataset during brain tumor resections. Brain shift related to loss of cerebrospinal fluid (CSF), brain dependency, edema, and tumor removal results in anatomical inaccuracies. Intraoperative MRI (iMRI) can be used to determine the extent of residual tumor burden and provide updated navigational data. Nevertheless, it requires highly constructive, logistic, and pecuniary effort associated with high costs and prolongation of the total operative time.¹¹ 5-ALA is a heme precursor that induces synthesis and accumulation of fluorescent protoporphyrin IX (PPIX) in malignant glioma but not in low-grade glioma tissues.¹¹ Intraoperative ultrasonography (IOUS) is a widely accessible, practical, and cost-effective imaging modality that provides real-time surgical guidance with minimal identified risks or

Received: May 27, 2019

Accepted: June 25, 2019

Published: August 8, 2019

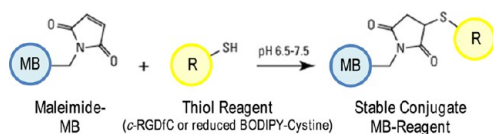


Figure 1. MB shell functionalization via thioether bonding: maleimide-MB is reacted with a sulfhydryl reagent (c-RGDfC or reduced BODIPY-cysteine).

additional operative time compared to other modalities. Accumulating data show a strong correlation between IOUS and postoperative MRI findings when evaluating the extent of tumor resection, suggesting that IOUS may have significant clinical implications. Furthermore, IOUS has the potential to compensate for brain shift due to CSF loss and tissue edema, which renders neuronavigation less reliable. Still, the difficult image interpretation is one of its major limitations.⁷ Therefore, in order to better visualize tumor borders and to improve resection completeness, an enhanced intraoperative ultrasound (US) image quality combined with direct microscopy visualization is highly desirable.

In glioblastoma, the MB's shell may allow for specific binding to the tumor vasculature. Also, the possibility to carry

drugs can make MBs a theranostic platform providing imaging and therapeutic treatment at the tumor site with the same device.⁶ Among endothelial cell receptors, $\alpha_v\beta_3$ integrin is considered a promising target for molecular imaging of cancer being expressed during angiogenesis,¹² a process necessary for malignant tumor growth and metastasis, as in the case of glioblastoma.^{13–15} The $\alpha_v\beta_3$ integrin binds arginine-glycine-aspartic acid (RGD) sequences of matrix proteins.¹⁶ As a result, the decoration of the MB surface with a cyclic analog of RGD may lead to selective adherence of MBs to the tumor microvessel endothelium and specific accumulation in the tumor site.¹⁵ MB lipid shells labeled with fluorophores, such as indocyanine green (ICG), can also offer the possibility for direct fluorescent visualization through an operative microscope.^{17,18} Thus, the lipid MBs would be able to support multi-modal tumor visualization, allowing for real-time intraoperative imaging during surgical resection via both US and in parallel fusion to the operative microscope.

In order to develop a compound for better visualization of tumor vasculature in humans, we assessed the biodistribution of MBs in the body of a rat model. Specifically, we investigated the biodistribution of a naked MB, the MB labeled with ICG (MB-ICG), the MB attached to RGD (MB-RGD), and the MB

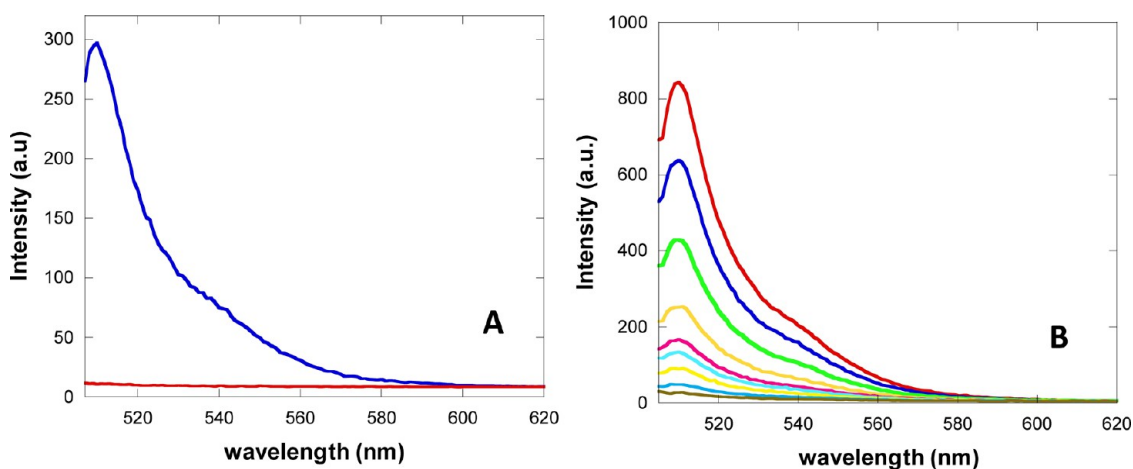


Figure 2. (A) Fluorescence spectra of disrupted lipid maleimide-MBs reacted with reduced BODIPY-cysteine (blue) and of naked lipid MBs as the control (red). (B) Fluorescence spectra of serial dilutions of a reduced BODIPY-cysteine standard solution (concentration range 0.01–0.45 μM). All measurements were carried out in PBS.

Table 1. Fluorescence Signal Observation

group no. and sex	test material	fluorescence signal observation (number observed/total number of animals)								
		eyes	brain	liver	stomach	spleen	intestine	colon	cecum	kidneys
1M	ICG (control item I)	6/6	5/6	6/6	5/6	5/6	6/6	0/6	0 ^a /6	6/6
2M	naked MBs (control item II)	0/6	0/6	0/6	0/6	0/6	0/6	0/6	0/6	0/6
3M	naked MBs-ICG (test item I)	6/6	6/6	6/6	6/6	6/6	6/6	0/6	0 ^b /6	6/6
4M	MBs-RGD (control item III)	0/6	0/6	0/6	0/6	0/5	0/6	0/5	0/6	0/6
5M	MBs-RGD-ICG (test item II)	6/6	6/6	6/6	6/6	6/6	6/6	0/6	0 ^b /6	6/6
group no. and sex	test material	fluorescence signal observation (number observed/total number of animals)								
		adrenals	urinary bladder	prostate	seminal vesicles	testis	sternum	heart	lungs	aorta
1 M	ICG (control item I)	5/6	5/6	5/6	5/6	5 ^c /6	5/6	5/6	5/6	0 ^d /6
2 M	naked MBs (control item II)	0/6	0/6	0/6	0/6	0/6	0/6	0/6	0/6	0/6
3 M	naked MBs-ICG (test item I)	6/6	6/6	6/6	6/6	6 ^e /6	6/6	6/6	6/6	0/6
4 M	MBs-RGD (control item III)	0/5	0/5	0/5	0/5	0/5	0/6	0/6	0/6	0/5
5 M	MBs-RGD-ICG (test item II)	6/6	6/6	6/6	6/6	6 ^e /6	6/6	6/6	6/6	0/6

^aSignal was detected in 3/6 rats in the vascular system surrounding the cecum. ^bSignal was detected in 6/6 rats in the vascular system surrounding the cecum. ^cSignal was detected in 1/6 rats in the testis and more pronounced in the vascular system surrounding the testis. ^dSignal was detected in 1/6 rats at the abdominal vena cava. ^eSignal was detected in 6/6 rats in the testis and more pronounced in the vascular system surrounding the testis.

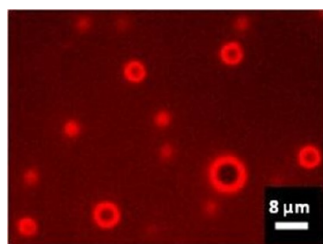


Figure 3. Wide-field NIR fluorescence of ICG-labeled lipid MBs, 60 \times oil immersion objective. The image was captured by a Nikon Inverted Microscope Eclipse Ti-E equipped with an LED source emitting at 770 nm (pE-100 LED, CoolLED Ltd., U.K.), a filter block containing an excitation filter, a dichroic beamsplitter (mirror) and a barrier/emission filter dedicated to ICG imaging (Chroma Technology, VT, U.S.A.), and a sCMOS camera (Zyla 4.2, Andor, U.K.).

labeled with ICG and attached to RGD (MB-RGD-ICG) following single intravenous (IV) injection to male Sprague Dawley rats.

MATERIALS AND METHODS

1,2-Distearoyl-*sn*-glycero-3-phosphocholine (DSPC), 1,2-dipalmitoyl-*sn*-glycero-3-phospho-(1'-*rac*-glycerol) sodium salt (DPPG-Na), and 1,2-distearoyl-*sn*-glycero-3-phosphoethanolamine-*N*-[maleimide(polyethylene glycol)-2000] ammonium salt (DSPE-PEG2000-Mal) were purchased from Avanti Polar Lipids. *tert*-Butanol (*t*-BuOH), palmitic acid (PA), poly(ethylene glycol) with a molecular weight of $M_r = 3500$ – 4500 (PEG 4000), ethylenediaminetetraacetic acid (EDTA), phosphate-buffered saline (PBS) at pH 7.4, and ethanol were from Sigma-Aldrich. BODIPY FL L-cystine and immobilized TCEP disulfide reducing gel were from Thermo Fisher Scientific. *Cyclo* (Arg-Gly-Asp-d-Phe-Cys), (*c*-RGDfC) peptide, was purchased from Peptides International and sulfur hexafluoride (SF_6) from Rivoira Gas and indocyanine green (ICG) from Pulsion Medical Systems. Human umbilical vein endothelial cells (HUVECs) in SupplementMix (Promocell) and HEPES buffered saline solution (HEPES-BSS) were from Promocell. μ -Slide I 0.4 ibiTreat and the Flow Through kit were from Ibidi. Water of Milli-Q purity grade (18.2 M Ω -cm) was produced with a deionization apparatus (Elga PureLab Classic).

MB Preparation. Targeted MB. MBs were synthesized as reported in Grossman et al.¹⁹ A lyophilized powder was prepared after dissolving in *tert*-butanol a mixture of 37.5 mol % DSPC, 37.5 mol % DPPG, 23 mol % PA, and 2 mol % DSPE-PEG2000-Mal together with PEG 4000. MBs were formed under a SF_6 atmosphere by dispersing in PBS an aliquot of the resultant powder; the suspension was manually shaken until a white homogeneous liquid was obtained.

After washing the bubbles from the lipid excess by centrifugation, the coupling reaction of maleimide-MBs with cysteine-tagged RGD (*c*-RGDfC) was carried out according to the scheme in Figure 1. Immediately before the coupling reaction, the peptide was reduced with TCEP (3.6 mM) to exclude possible disulfide bonds between cysteine residues of *c*-RGDfC. After that, MBs were reacted for 1 h at 4 $^{\circ}C$ in PBS-containing EDTA (5 mM) with an amount of *c*-RGDfC corresponding to 10 times the moles of DSPE-PEG2000-Mal in the MB sample. Targeted MBs-RGDs were washed from the unbound peptide by three rounds of centrifugation and stored as lyophilized powder. After each centrifugation step, MBs-RGDs were resuspended in PBS-containing 10% w/v maltose as a cryoprotectant.

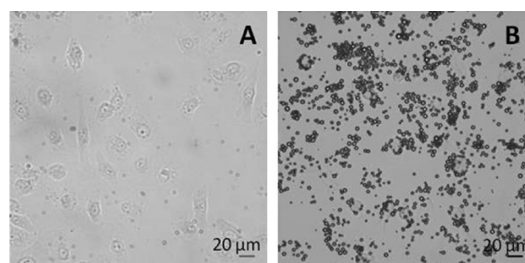


Figure 4. Adhesion of *c*-RGDfC-targeted MBs onto HUVECs under flow conditions (1 dyne/cm²; transmission mode, 40 \times objective). (A) naked MBs; (B) RGD-MBs.

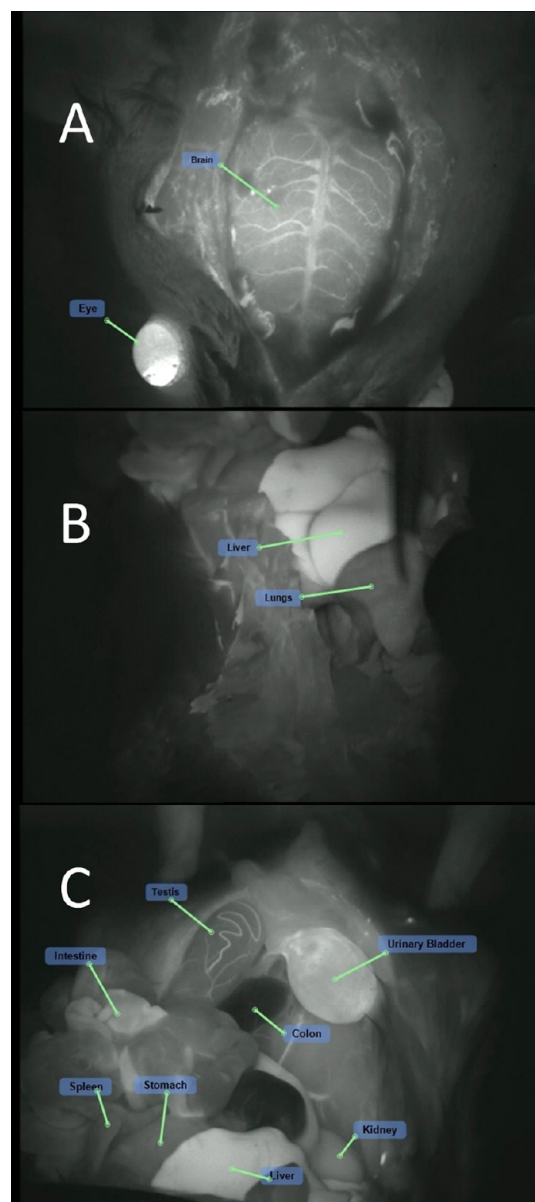


Figure 5. ICG treatment (group 1M): fluorescence visualization of the (A) cranium, (B) chest cavity, and (C) peritoneal cavity following ICG injection.

Naked MBs. Nonfunctionalized, plain lipid MBs (naked MBs) were prepared as the control test items by omitting the coupling reaction with the peptide. In this case, DSPE-PEG2000-Mal was not present in the lipid mixture in *tert*-butanol.

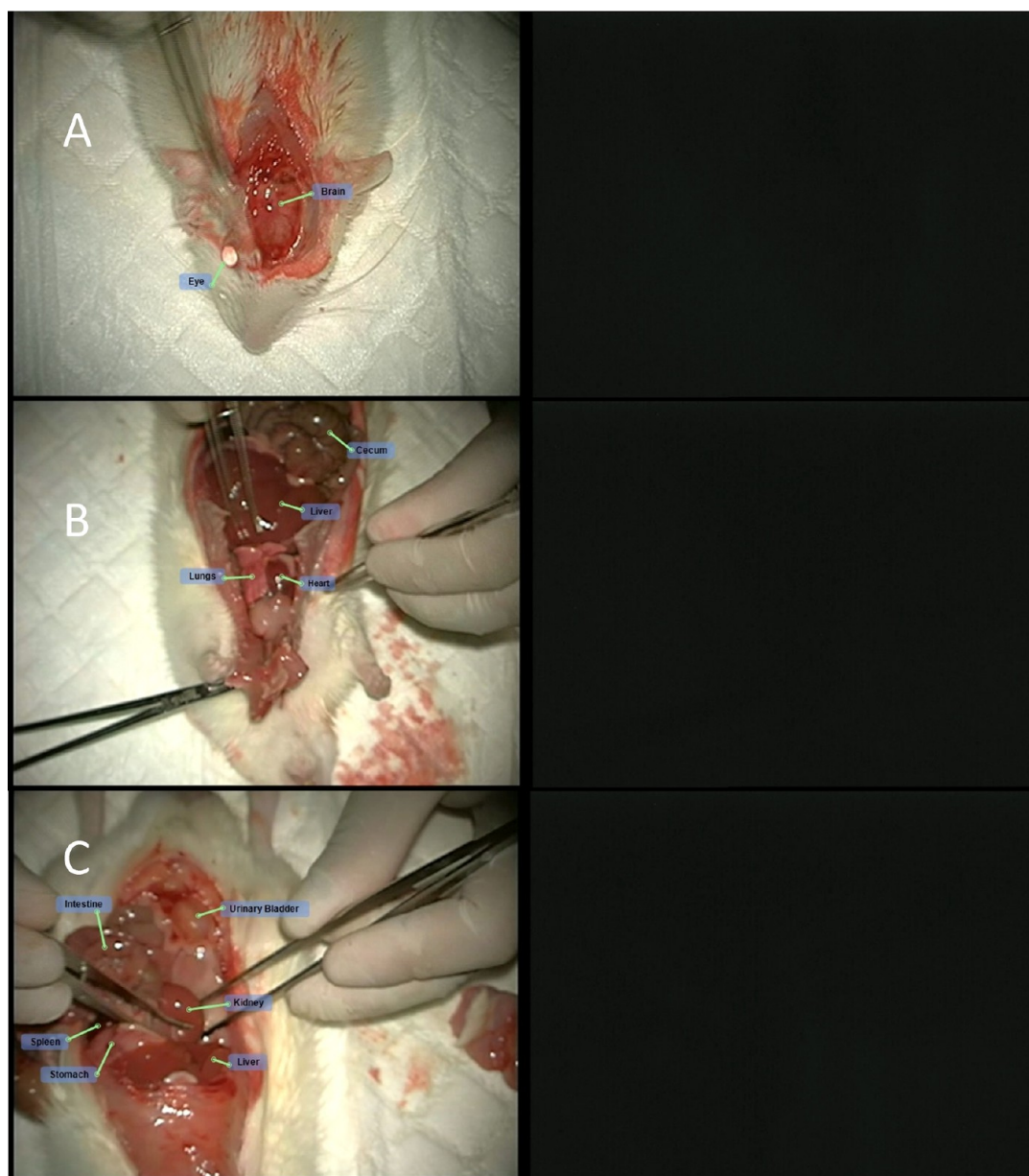


Figure 6. Naked MBs treatment (group 2M): white light (left) and fluorescence (right) visualization of the (A) cranium, (B) chest cavity, and (C) peritoneal cavity following naked-MBs injection.

MB Reconstitution and ICG Labeling. All lyophilized samples of naked MBs and MBs-RGD were reconstituted on the spot on the day of the experiment. In order to do this, before adding the carrier liquid (5 mL of saline), the headspace of each sample vial was filled with SF₆. Then, the bubbles were formed by manually shaking the resulting suspension in the presence of SF₆. MBs-ICG and MBs-RGD-ICG were prepared by adding to the MB powder in contact with SF₆ the fluorescent probe solution first (1 mL of ICG, 5 mg/mL, in water) and then saline up to 5 mL of the final sample volume. Each vial of fresh reconstituted MBs resulted in an MB suspension of $\sim 10^8$ MBs/mL.

Ligand Determination on MBs. The amount of attached peptide onto the MB shell via thioether bonding was evaluated in an indirect way by replacing, during the coupling reaction, *c*-RGDfC with a cysteine carrying fluorescent probe, the reduced form of BODIPY-cystine (see Figure 1). After

BODIPY-cystine reduction with TCEP, the conjugation reaction with maleimide-bearing MBs was carried out following the very same procedure used for *c*-RGDfC. The yield of MB shell modification was evaluated by measuring the fluorescence of the suspension of BODIPY-MBs disrupted by sonication and comparing the resulting signal with that from dilutions of a reduced BODIPY-cystine solution (Figure 2) using an RF-5301 Shimadzu spectrofluorimeter (Shimadzu, Rome, Italy) (excitation and emission slit widths, 1.5 nm; in “high” sensitivity mode). In order to assess the extent of shell modification per MB, the concentration of bubble samples as the number of MBs per milliliter of the MB suspension was determined by optical microscopy before MB disruption by sonication using a Neubauer chamber.

Parallel Plate Flow Chamber Adhesion Assay. HUVECs were cultured in the supplemented endothelial cell growth medium at 37 °C in a 5% CO₂/95% air humidified

atmosphere. Flow chamber slides (μ -Slides I 0.4, Ibidi) were coated with 2% gelatin solution then 2.5×10^5 HUVECs were seeded. The μ -Slides were put upside down in the incubator (HeraCell 150i, Thermo Fisher Scientific) and left in this position overnight to allow cells to grow and adhere on the roof of the chamber slides. Afterward, cells were washed three times with PBS and placed in an upright position under an inverted microscope (Nikon Inverted Microscope Eclipse Ti-E, Florence, Italy) equipped with a 40 \times objective (Nikon, Japan), a motorized stage, and the Zyla sCMOS camera 4.2 (Andor, Belfast, U.K.) for video recording. Nontargeted plain bubbles and *c*-RGDfC functionalized lipid MBs (10^6 MBs/mL) were pumped into the channel slide with a syringe pump at a constant flux of 0.76 mL/min, corresponding to a shear stress of 1 dyn/cm². After 10 min, five different fields of view were captured using bright field microscopy (Nikon NIS-Element AR, Florence, Italy). Then, the channel slide was inverted upside down for 5 min, placed upright under the microscope, and perfused further for 10 min with PBS to wash out the unspecifically adhered and easily detachable MBs. Pictures corresponding to five different fields of view were captured again.

Animals. Seven-week-old male Sprague Dawley rats weighing 205 g (183–226 g) were obtained from Envigo RMS, Israel. All dosing solutions were injected by single IV injection into one of the animal's tail veins. Test items and saline controls were injected in volume doses of 4 mL/kg corresponding to 692 mg/kg of formulations containing naked MBs, MBs labeled with indocyanine green (MB-ICG) for visualization, MBs conjugated to a cyclic molecule containing the tripeptide Arg-Gly-Asp (RGD), and MBs labeled RGD and ICG (MB-RGD-ICG). The animals were observed for a total duration of up to 15 min post dosing (Table 1). The identification of the MB in various organs was monitored by fluorescence microscopy in anesthetized animals as well as real-time US for brain imaging. Equally sized control groups under identical conditions were used in this study. One control group was used to establish fluorescence background conditions (ICG), and two control groups were used to test autofluorescence from the test items (MBs and MB-RGD). This study was performed following an application form review by the National Council for Animal Experimentation and after receiving approval (no. 15–06-182) that the study complies with the rules and regulations set forth.

Fluorescence Imaging. Following each surgical procedure, animals were placed in a suitable recumbence to allow visualization of ICG using a Pentero classic surgical microscope (OPMI Pentero flow 800, Carl Zeiss, Meditec AG, Jena, Germany) equipped with an IR800 functionality, and representative images were taken for evaluation.

Ultrasound Imaging. Ultrasound imaging was used on all animals in the study to visualize the blood flow in the brain. A Mindray M9 ultrasound machine (Mindray Co, ShenZhen, China) connected to a linear array (6–14 MHz) transducer was used.

Termination. At termination of the study, animals were euthanized by severing of the heart.

Data Evaluation. Evaluation of the presence or absence of MBs in the examined tissues was based on assessing the difference between the fluorescence pattern and intensity of a test item compared to the fluorescence pattern and intensity of a control item. The autofluorescence observed in a respective control item was taken into account (tested MB without ICG).

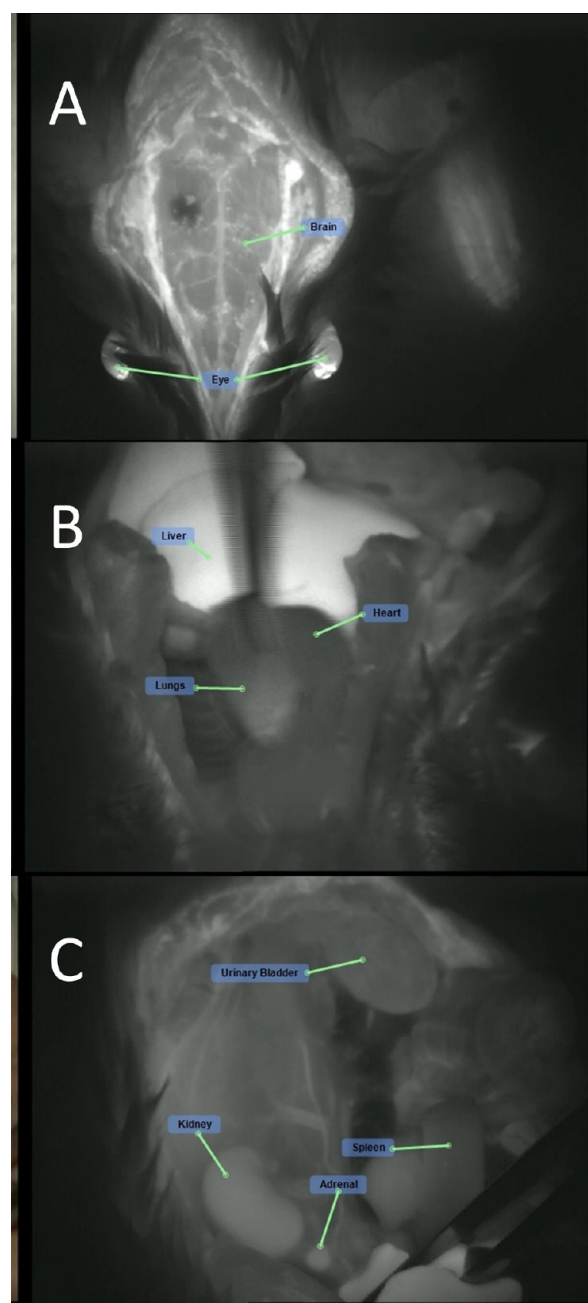


Figure 7. Naked MBs-ICG treatment (group 3M): fluorescence visualization of the brain and eye following naked MBs-ICG injection: (A) cranium, (B) chest cavity, and (C) peritoneal cavity.

RESULTS

Characterization of MB Contrast Agents. All of the MBs used in this study had a mean diameter of approximately 2.8 μ m with less than 2% of a diameter above 9 μ m. Figure 3 is a fluorescence image of reconstituted lipid MBs after ICG labeling showing accumulation of the fluorescent dye on the shells.

The feasibility of surface functionalization of maleimide-bearing MBs via thioether bonding with the thiol carrying ligand *c*-RGDfC was probed with the fluorescent marker BODIPY-cystine. By this way the extent of conjugation was evaluated with fluorescence spectroscopy resulting in 1.9×10^6 molecules of ligands per MB. Since the MB concentration after bubble reconstitution is 2.5×10^8 MBs/mL, a volume dose of

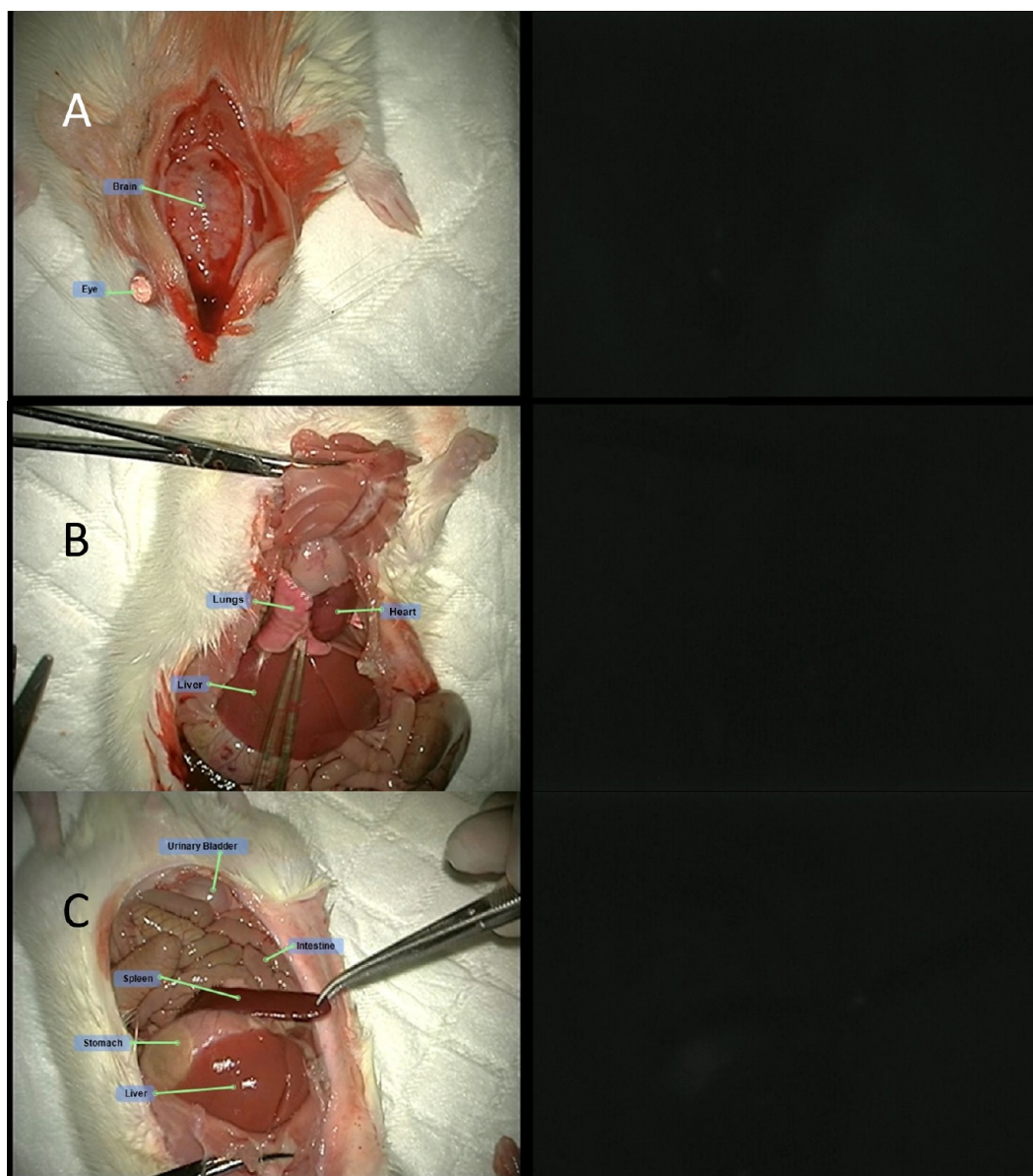


Figure 8. MBs-RGD treatment (group 4M): white light (left) and fluorescence (right) visualization following MBs-RGD injection of (A) cranium, (B) chest cavity, (C) peritoneal cavity.

4 mL/kg of the test item corresponds to a dose of the peptide of 2 $\mu\text{g}/\text{kg}$. The success of shell functionalization with *c*-RGDfC was confirmed by testing the functional adhesion of targeted MBs in a parallel plate flow chamber experiment. HUVECs were chosen as the positive control cell line for $\alpha_v\beta_3$ expression, the integrin recognized by the Arg-Gly-Asp sequence presented by the surface of the modified lipid MBs. The cells were grown on the upper wall of the chamber slide in order to guarantee optimal exposure conditions for contact with floating bubbles. Figure 4 shows the MB adhesion after 10 min of infusion of fresh PBS washing out nonfirmly and unspecifically bound MBs: RGD-MBs allowed efficient targeting of $\alpha_v\beta_3$ integrin-expressing cells (16.7 ± 2.2 RGD-MBs/HUVEC).

These results and the favorable outcome of the toxicological studies¹⁹ demonstrate that the prepared functionalized MBs have the potential to be useful as a dual-modal targeted contrast agent. The next step was therefore to investigate the biodistribution in the body and especially in the brain of rats.

Animal Studies. No treatment-related mortality occurred in any of the animals throughout the entire observation period. All groups had a comparable group mean body weight at dosing.

Fluorescence Biodistribution. Slight autofluorescence was seen in the nonglandular stomach (forestomach) and in the eyes of animals injected with no fluorescence marker (ICG). This autofluorescence had a markedly lower intensity compared to the intensity seen in organs from animals injected with ICG. ICG was detected in the following organs of all animals injected with ICG alone or ICG with MBs (naked and RGD): eyes, brain, liver, stomach, spleen, intestine, kidneys, adrenals, urinary bladder, prostate, seminal vesicles, testis, sternum, heart, and lungs. Additionally, the vascular system surrounding the cecum and testis was also visualized by fluorescence. A fluorescence signal was detected with the greatest intensity in the liver and the eyes, to a lesser intensity in the kidneys, adrenal, intestine, brain, and lungs, and at low intensity in the rest of the organs listed above. The pattern,

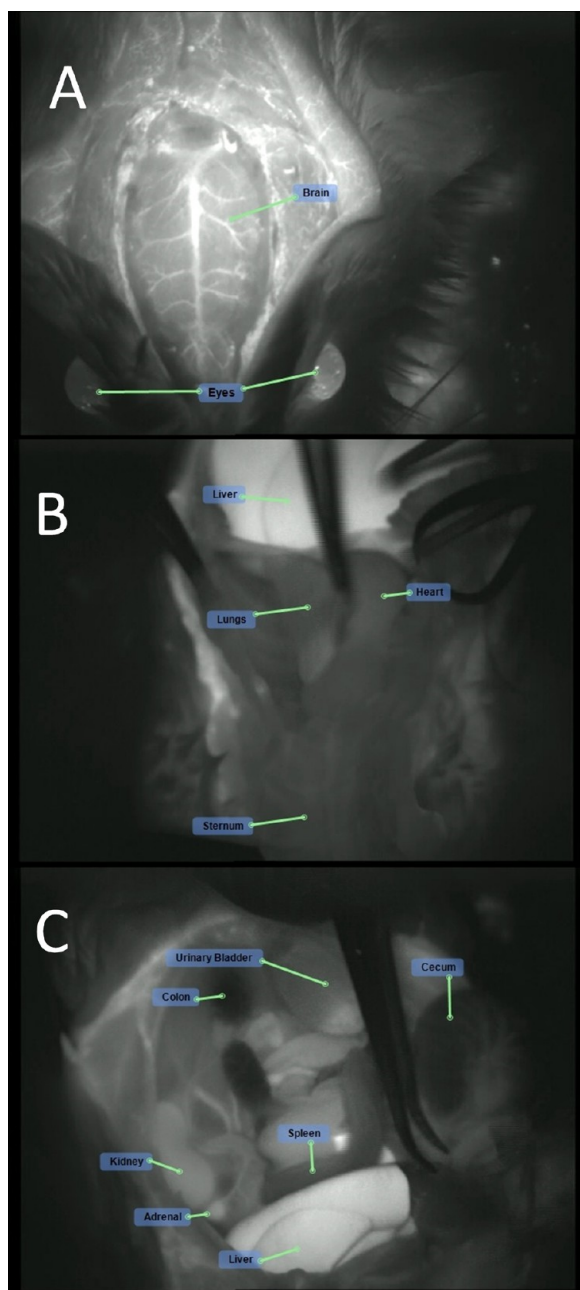


Figure 9. MBs-RGD-ICG treatment (group 5M): fluorescence visualization following MBs-RGD-ICG injection of the (A) cranium, (B) chest cavity, and (C) peritoneal cavity.

duration, and intensity of the fluorescence signal could not be differentiated between animals treated with ICG alone and animals treated with MBs, MBs-ICG or MBs-RGD-ICG (Table 1). Representative photos of different organs in both white light and fluorescence following the different treatments are presented below (Figures 5–9).

Ultrasound Biodistribution. Following MB injection (either naked or RGD), there was a sharp rise in the Doppler signal within seconds of injection. The signal was mainly located at the choroid plexus, septum pellucidum, and the meninges in the brain. The signal subsided within a few minutes. Following a saline injection to the same respective animal (several minutes after test item injection in all MB-containing test items, i.e., groups 2M–5M), the rise in the Doppler signal was not observed. Additionally, following ICG injection alone (group



Figure 10. Ultrasound post injection visualization of the brain following (A) ICG injection, (B) naked MBs injection, and (C) saline injection.

1M), no sharp rise in the Doppler signal was observed, and the signal was equivalent to that seen in following saline injections (Figures 10–13).

DISCUSSION

Recent advances in the field of neuroimaging and the development of novel MBs have improved the options for real-time imaging during brain surgery. Many engineered nano- and microparticles, including MBs, can be easily manipulated to serve as an imaging agent as well as for drug delivery, especially in the setting of brain surgery.

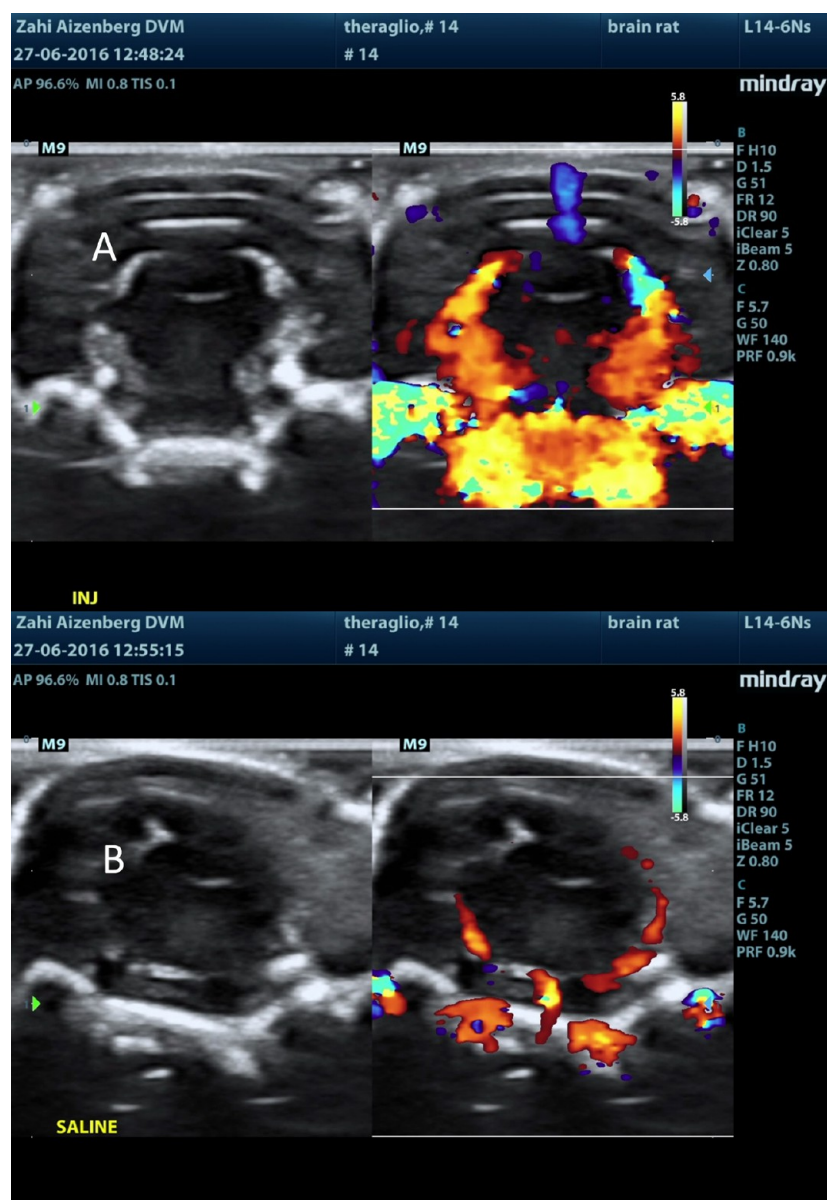


Figure 11. Naked MBs-ICG treatment (group 3M): ultrasound post injection visualization of the brain following (A) naked MBs-ICG injection and (B) saline injection.

Reported here is the whole body biodistribution in rats after IV injection of lipid MBs with a modified shell surface suitable for tumor vasculature targeting and NIR fluorescence imaging. The engineered MBs used in this study included bubbles physically labeled with the NIR probe ICG and covalently conjugated with the tumor-targeting peptide *c*-RGDFc with a relatively narrow size range ($\pm 1 \mu\text{m}$) and are well dispersed, thus facilitating the IV administration. Preliminary studies using the peptide motif have been performed, and results suggest the strategy to be safe and specific.¹⁶

In fact, we have just recently investigated the potential toxicity of these MB compounds *in vivo*.¹⁹ Following IV injections of two doses of plain MBs and MBs engineered for targeting and NIR fluorescence visualization, animals were closely monitored for potential acute and chronic responses. No mortality occurred during the study period in any of the dosing groups. Body weights were stable during the study period. Minor, mostly reversible changes in hematological and biochemical analyses were observed in some of the treated animals. All

changes were reversible after 7 days. Histopathology examination in the high-dose animals showed development of foreign body granulomatous inflammation, and we concluded that the low-dose tested items appear to be safe. Furthermore, the *in vitro* studies demonstrated that the targeted MBs are able to functionally adhere onto cell substrates expressing the proper receptor. Accordingly, we proceeded with the low-dose tested items to test its efficacy.

Due to the relatively short half-life of MBs,²⁰ the 15 min time point was chosen to best represent initial uptake in individual internal organs. Our results show a rapid uptake of both the test and control items in the liver, and a pattern was found also for free ICG^{21,22} and in other studies on MBs.^{20,23,24} The US results, directly linked to the presence of MBs registered in the brain, were compared to those of the intraoperative microscope with the IR filter and confirmed that the engineered MBs rapidly reach the brain. In targeted US imaging, it is crucial that the US imaging signal from MBs suitably modified with a marker for functional adhesion can be

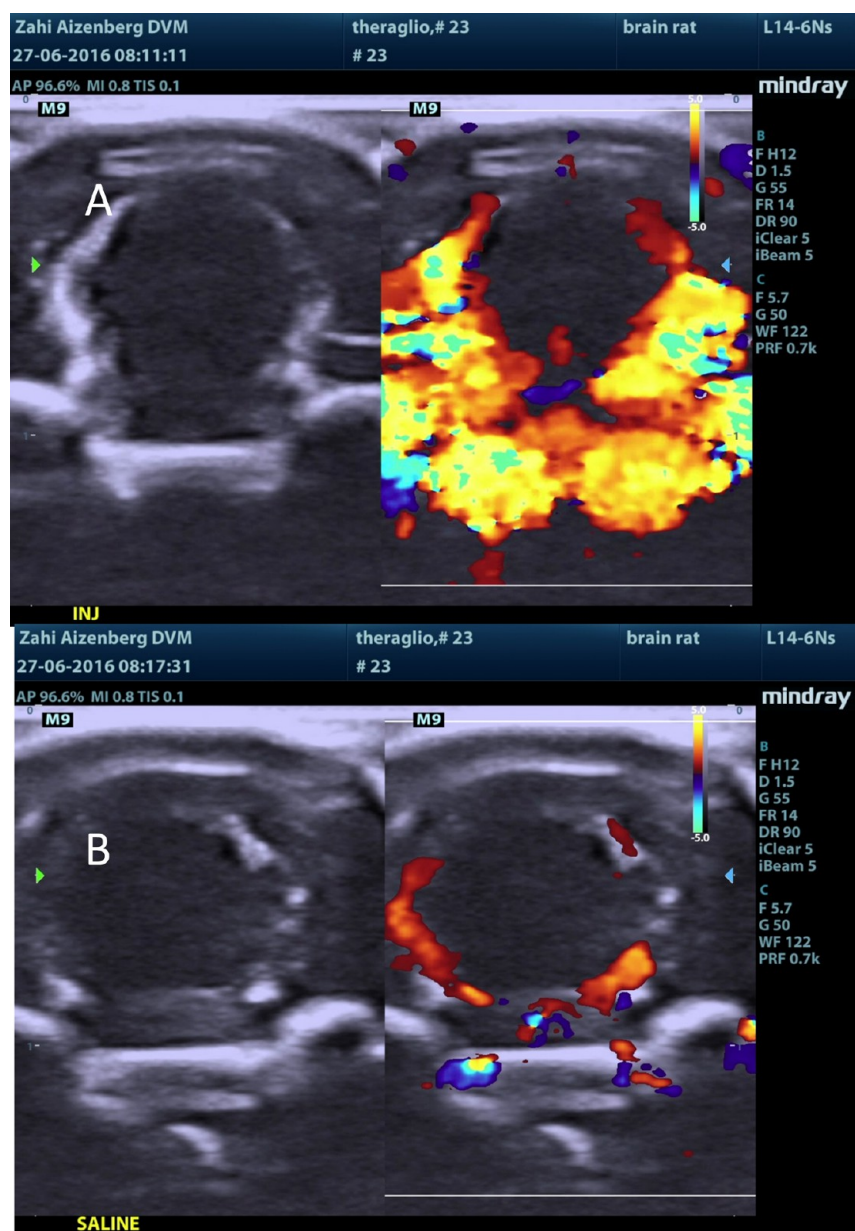


Figure 12. MBs-RGD treatment (group 4M): ultrasound post injection. Ultrasound visualization of the brain following (A) MBs-RGD injection and (B) saline injection.

differentiated from the background imaging signal. This is a challenge in tissues with a high level of nonspecific MB accumulation.²⁰ In our case, the fluorescence signal in the organs besides the liver, such as in the brain, was moderate suggesting that a specific signal from a tumor vasculature could be obtained by targeted imaging using a dedicated US sequence, with the background distribution level of targeted MBs being low in the surrounding normal tissue.

One limitation of our biodistribution study was that we did not covalently anchor ICG to MB surfaces, and as a consequence, the fluorescence signal visualized by using the surgical microscope came not only from the physically adsorbed labeled ICG-MBs but also from the injected medium as free ICG. We opted for the NIR dye ICG, taking advantage of the ability of ICG to incorporate stably into lipid membranes,²⁵ its detection even in deeper tissues during the operation, its ability of improving the recognition of residual microtumors during surgical operations, and the fact that it is

an FDA/EMA-approved molecule for use in humans. Moreover, since lipid MBs are already EMA-approved for use in humans, we postulated that the potential final microdevice formulation, which includes functional modified lipid MBs physically labeled with ICG, would be more easily translated into the clinical arena.

CONCLUSIONS

Following single IV administrations of the test items MB-ICG and MB-RGD-ICG to male Sprague Dawley rats, the test items are present in the brain. These data were confirmed by both US imaging, which is specific for MBs, and by NIR fluorescence imaging. It is likely that the test items are also distributed to other tissues with a rapid uptake by the liver; however, because of the limitations of the imaging techniques and the presence of free dye in the labeled MBs samples, biodistribution to other organs cannot be proven. From the

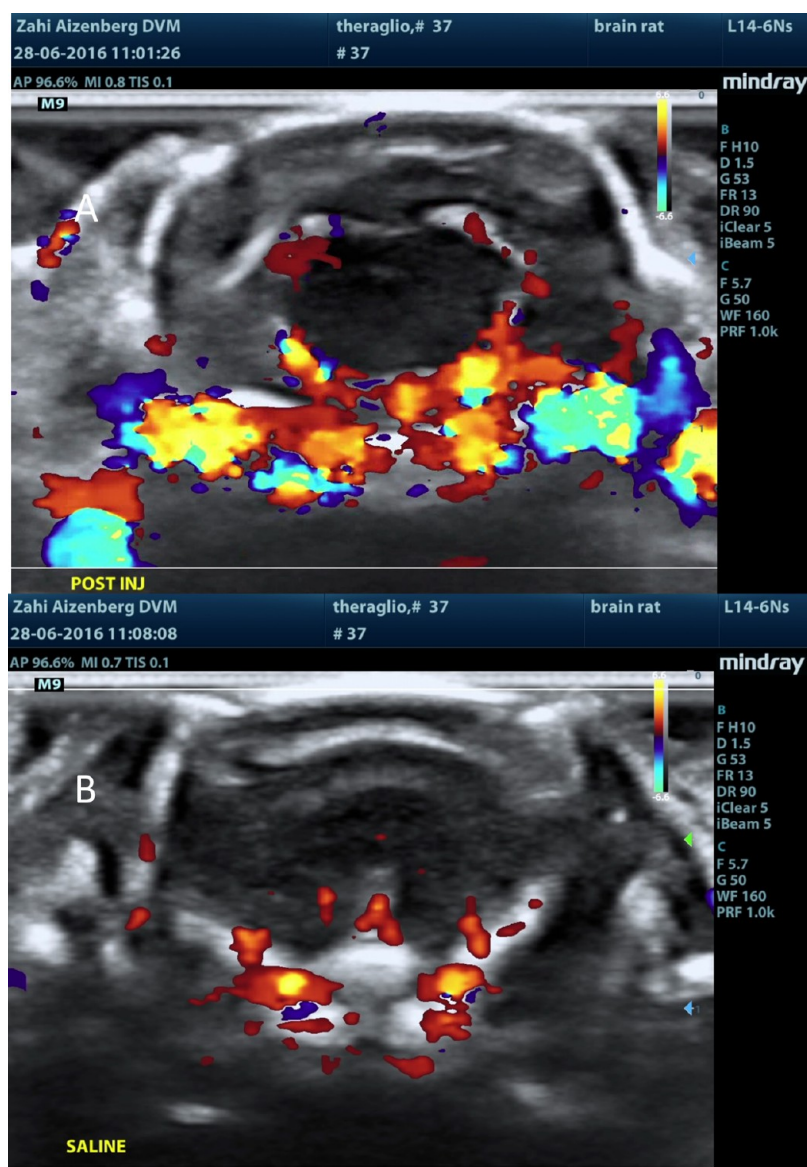


Figure 13. MBs-RGD-ICG treatment (group 5M): ultrasound post injection. Ultrasound visualization of the brain following (A) MBs-RGD-ICG injection and (B) saline.

data on *in vivo* whole-body biodistribution of lipid MBs reported in the literature, we can hypothesize a similar fate also for the MBs presented in this work. According to this, upon injection, MBs circulate within the vascular system due to size and deformability similar to that of erythrocytes. Their persistence in the blood circulation depends on the dissolution rate of the gaseous core and on the rate of clearance by the mononuclear phagocyte system. *In vivo* imaging studies revealed that increasing the microbubble diameter and/or concentration significantly increases circulation persistence from ca. 1.5 min for 2 μm -sized bubbles to 6 min for 6 μm -sized bubbles.²⁶ Six minutes is reported also as the elimination half-life of the marketed UCA Sonovue.²⁷ Further, dynamic micropositron emission tomography (micro-PET) in living mice of lipid-shelled MBs targeted to tumor angiogenesis-related vascular endothelial growth factor (VEGF) receptor 2 (VEGFR2) demonstrated that 50% of targeted MBs cleared after approximately 3.5 min, and approximately 95% were cleared from the blood circulation after 30 min with a rapid uptake and retention of targeted MBs in both the liver and spleen.²⁰ Several

studies demonstrated significant accumulation of lipid-shelled MBs in the liver and spleen with some variation according to the animal model and microbubble construct. This retention is most likely due to phagocytosis by Kupffer cells in the liver and by macrophages and the mononuclear phagocyte system in the spleen.^{20,28} Finally, we cannot exclude pulmonary macrophage contribution in lung clearance and also pulmonary entrapment of MBs with a diameter greater than 5 μm . Intravital microscopy studies revealed that the majority of entrapped lipid MBs became ellipsoidal indicating that microvascular entrapment is a transient phenomenon due to MB deformability with 85% of MBs dislodged by 10 min and no adverse hemodynamic effects.²⁹ Then, when the microbubble shell collapses, the relatively inert gas (perfluorocarbon gases or SF_6) is released into the plasma and exhaled via the lungs.²⁷

In conclusion, after IV injection, the use of the MBs was safe with no treatment-related mortality occurring in any of the animals throughout the entire observation period. Furthermore, the ability of MBs to localize in the brain opens the possibility to test the efficacy of targeted MBs performing

future US molecular imaging experiments in a rat brain tumor model.

AUTHOR INFORMATION

Corresponding Author

*E-mail: rachelgr@tasmc.health.gov.il. Phone: +972-3-6974273. Fax: +972-3-6974860.

ORCID

Gaio Paradossi: 0000-0003-3051-3811

Rachel Grossman: 0000-0001-7741-375X

Notes

The authors declare no competing financial interest.

ACKNOWLEDGMENTS

This work was funded by the EU Seventh Framework Programme FP7/2007-2013 "TheraGlio" (grant agreement no. 602923).

REFERENCES

- (1) Bauchet, L.; Ostrom, Q. T. Epidemiology and Molecular Epidemiology. *Neurosurg. Clin. N. Am.* **2019**, *30*, 1–16.
- (2) Stupp, R.; Mason, W. P.; van den Bent, M. J.; Weller, M.; Fisher, B.; Taphoorn, M. J. B.; Belanger, K.; Brandes, A. A.; Marosi, C.; Bogdahn, U.; Curschmann, J.; Janzer, R. C.; Ludwin, S. K.; Gorlia, T.; Allgeier, A.; Lacombe, D.; Cairncross, J. G.; Eisenhauer, E.; Mirimanoff, R. O. Radiotherapy plus concomitant and adjuvant temozolomide for glioblastoma. *N. Engl. J. Med.* **2005**, *352*, 987–996.
- (3) Ostrom, Q. T.; Gittleman, H.; Truitt, G.; Boscia, A.; Kruchko, C.; Barnholtz-Sloan, J. S. CBTRUS Statistical Report: Primary Brain and Other Central Nervous System Tumors Diagnosed in the United States in 2011-2015. *Neuro Oncol.* **2018**, *20*, iv1–iv86.
- (4) Grossman, R.; Shimony, N.; Shir, D.; Gonen, T.; Sitt, R.; Kimchi, T. J.; Harosh, C. B.; Ram, Z. Dynamics of FLAIR Volume Changes in Glioblastoma and Prediction of Survival. *Ann. Surg. Oncol.* **2017**, *24*, 794–800.
- (5) Kiessling, F.; Fokong, S.; Bzyl, J.; Lederle, W.; Palmowski, M.; Lammers, T. Recent advances in molecular, multimodal and theranostic ultrasound imaging. *Adv. Drug Delivery Rev.* **2014**, *72*, 15–27.
- (6) Nakada, M.; Nambu, E.; Furuyama, N.; Yoshida, Y.; Takino, T.; Hayashi, Y.; Sato, H.; Sai, Y.; Tsuji, T.; Miyamoto, K. I.; Hirao, A.; Hamada, J. I. Integrin $\alpha 3$ is overexpressed in glioma stem-like cells and promotes invasion. *Br. J. Cancer* **2013**, *108*, 2516–2524.
- (7) Prada, F.; Del Bene, M.; Mattei, L.; Casali, C.; Filippini, A.; Legnani, F.; Mangraviti, A.; Saladino, A.; Perin, A.; Richetta, C.; Vetrano, I.; Moiraghi, A.; Saini, M.; DiMeco, F. Fusion imaging for intra-operative ultrasound-based navigation in neurosurgery. *J. Ultrasound* **2014**, *17*, 243–251.
- (8) Sanai, N.; Polley, M. Y.; McDermott, M. W.; Parsa, A. T.; Berger, M. S. An extent of resection threshold for newly diagnosed glioblastomas. *J. Neurosurg.* **2011**, *115*, 3–8.
- (9) Senft, C.; Bink, A.; Franz, K.; Vatter, H.; Gasser, T.; Seifert, V. Intraoperative MRI guidance and extent of resection in glioma surgery: a randomised, controlled trial. *Lancet Oncol.* **2011**, *12*, 997–1003.
- (10) Stummer, W.; Pichlmeier, U.; Meinel, T.; Wiestler, O. D.; Zanella, F.; Reulen, H. J.; Group, A. L.-G. S. Fluorescence-guided surgery with 5-aminolevulinic acid for resection of malignant glioma: a randomised controlled multicentre phase III trial. *Lancet Oncol.* **2006**, *7*, 392–401.
- (11) Hollon, T.; Stummer, W.; Orringer, D.; Suero Molina, E. Surgical Adjuncts to Increase the Extent of Resection. *Neurosurg. Clin. N. Am.* **2019**, *30*, 65–74.
- (12) Brooks, P. C.; Clark, R. A.; Cheresch, D. A. Requirement of vascular integrin $\alpha v \beta 3$ for angiogenesis. *Science* **1994**, *264*, 569–571.
- (13) Folkman, J. Role of angiogenesis in tumor growth and metastasis. *Semin. Oncol.* **2002**, *29*, 15–18.
- (14) Hannah, A.; Luke, G.; Wilson, K.; Homan, K.; Emelianov, S. Indocyanine green-loaded photoacoustic nanodroplets: dual contrast nanoconstructs for enhanced photoacoustic and ultrasound imaging. *ACS Nano* **2014**, *8*, 250–259.
- (15) Xu, R. X.; Huang, J.; Xu, J. S.; Sun, D.; Hinkle, G. H.; Martin, E. W.; Pivoski, S. P. Fabrication of indocyanine green encapsulated biodegradable microbubbles for structural and functional imaging of cancer. *J. Biomed. Opt.* **2009**, *14*, No. 034020.
- (16) Danhier, F.; Le Breton, A.; Pr eat, V. RGD-based strategies to target $\alpha v \beta 3$ integrin in cancer therapy and diagnosis. *Mol. Pharmaceutics* **2012**, *9*, 2961–2973.
- (17) Frazier, K. S.; Seely, J. C.; Hard, G. C.; Betton, G.; Burnett, R.; Nakatsuji, S.; Nishikawa, A.; Durchfeld-Meyer, B.; Bube, A. Proliferative and nonproliferative lesions of the rat and mouse urinary system. *Toxicol. Pathol.* **2012**, *40*, 14S–86S.
- (18) Huveneers, S.; Truong, H.; Danen, E. H. J. Integrins: signaling, disease, and therapy. *Int. J. Radiat. Biol.* **2007**, *83*, 743–751.
- (19) Paradossi, G.; Oddo, L.; Cerroni, B.; Ben-Harush, C.; Ariel, E.; Di Meco, F.; Ram, Z.; Grossman, R. In Vivo Toxicity Study of Engineered Lipid Microbubbles in Rodents. *ACS Omega* **2019**, *4*, 5526–5533.
- (20) Willmann, J. K.; Cheng, Z.; Davis, C.; Lutz, A. M.; Schipper, M. L.; Nielsen, C. H.; Gambhir, S. S. Targeted microbubbles for imaging tumor angiogenesis: assessment of whole-body biodistribution with dynamic micro-PET in mice. *Radiology* **2008**, *249*, 212–219.
- (21) Desmettre, T.; Devoisselle, J. M.; Mordon, S. Fluorescence properties and metabolic features of indocyanine green (ICG) as related to angiography. *Surv. Ophthalmol.* **2000**, *45*, 15–27.
- (22) Cherrick, G. R.; Stein, S. W.; Leevy, C. M.; Davidson, C. S. Indocyanine green: observations on its physical properties, plasma decay, and hepatic extraction. *J. Clin. Invest.* **1960**, *39*, 592–600.
- (23) Perkins, A. C.; Frier, M.; Hindle, A. J.; Blackshaw, P. E.; Bailey, S. E.; Hebden, J. M.; Middleton, S. M.; Wastie, M. L. Human biodistribution of an ultrasound contrast agent (Quantison) by radiolabelling and gamma scintigraphy. *Br. J. Radiol.* **1997**, *70*, 603–611.
- (24) Walday, P.; Tolleshaug, H.; Gjoen, T.; Kindberg, G. M.; Berg, T.; Skotland, T.; Holtz, E. Biodistributions of air-filled albumin microspheres in rats and pigs. *Biochem. J.* **1994**, *299*, 437–443.
- (25) Kraft, J. C.; Ho, R. J. Interactions of indocyanine green and lipid in enhancing near-infrared fluorescence properties: the basis for near-infrared imaging in vivo. *Biochemistry* **2014**, *53*, 1275–1283.
- (26) Sirsi, S.; Feshitan, J.; Kwan, J.; Homma, S.; Borden, M. Effect of microbubble size on fundamental mode high frequency ultrasound imaging in mice. *Ultrasound Med. Biol.* **2010**, *36*, 935–948.
- (27) Schneider, M. Characteristics of SonoVue. *Echocardiography* **1999**, *16*, 743–746.
- (28) Warram, J. M.; Sorace, A. G.; Mahoney, M.; Samuel, S.; Harbin, B.; Joshi, M.; Martin, A.; Whitworth, L.; Hoyt, K.; Zinn, K. R. Biodistribution of P-selectin targeted microbubbles. *J. Drug Targeting* **2014**, *22*, 387–394.
- (29) Lindner, J. R.; Song, J.; Jayaweera, A. R.; Sklenar, J.; Kaul, S. Microvascular rheology of Definity microbubbles after intra-arterial and intravenous administration. *J. Am. Soc. Echocardiogr.* **2002**, *15*, 396–403.